

The covariation between Mg—C isotopes and trace elements in dolostones: Implications for reconstructing the seawater chemistry



Zhongya Hu ^{a,*}, Zhong Han ^c, Anlin Ma ^b, Zhiqiang Xia ^{b,c}, Lichao Wang ^d, Weiqiang Li ^b

^a State Key Laboratory of Marine Geology, Tongji University, Shanghai 200092, China

^b State Key Laboratory for Mineral Deposits Research, School of Earth Sciences and Engineering, Nanjing University, Nanjing, Jiangsu 210093, China

^c State Key Laboratory of Oil and Gas Reservoir Geology and Exploitation, Institute of Sedimentary Geology, Chengdu University of Technology, Chengdu 610059, China

^d State Key Laboratory of Oil and Gas Reservoir Geology and Exploitation, School of Geoscience and Technology, Southwest Petroleum University, Chengdu, Sichuan 610500, China

ARTICLE INFO

Article history:

Received 19 September 2023

Received in revised form 23 November 2023

Accepted 23 November 2023

Available online 1 December 2023

Editor: Dr. Brian Jones

Keywords:

Magnesium isotopes
Dolomite
Dolomitization
Seawater geochemistry
Coupling effects

ABSTRACT

Magnesium isotopes of marine dolomites have the potential to reconstruct the Mg isotopic signals of coeval seawater. However, a massive dolostone sequence can form via the coupling effects of multiple dolomitization events, which can potentially reset the Mg isotopic compositions of dolomites during each migration of the dolomitization fluid. How to distinguish changes of seawater chemistry and early diagenetic effects which have been recorded in dolomites is crucial for the reconstruction of seawater Mg isotopic signals. Here we studied the Mg-Sr-C-O isotope systematics and trace elements of a dolostone sequence from the Qiangtang Basin in the hinterland of Tibet. Multiple lines of evidence consistently indicate the lack of deep-burial diagenesis and high-temperature alteration in the carbonates. The stratigraphic variations of isotopic and elemental compositions of the dolostone profile are generally characterized by the co-variation between Mg—C isotopes and trace element contents. Our modeling results indicated that a single downward dolomitization can cause the large Mg isotopic variability of dolomites, ca. 1 ‰, within a dolomitization front. However, when the limestones in the profile were completely dolomitized, the coupling effects of multiple downward dolomitizations will homogenize the $\delta^{26}\text{Mg}$ values of dolostones. Therefore, we attribute the observed co-variation in isotopic and elemental signals in the dolostone sequence to the changes in the chemistry of evolved seawater within the platform. The reconstructed seawater $\delta^{26}\text{Mg}$ values from the Carnian to Early Jurassic are lower than previous model-based estimations. This result implies an overestimation of the production of shallow-water carbonate in literature during Late Triassic to Early Jurassic. Our study highlights the importance of utilizing multiple geochemical proxies to identify the controlling factors driving Mg isotope variability in dolomites.

© 2023 Elsevier B.V. All rights reserved.

1. Introduction

The geochemical changes of marine carbonates have been extensively studied for tracing the geological events recorded in rocks (Gregg et al., 1992; Swart, 2015; Hohl and Viehmann, 2021; Immenhauser, 2022). In the last decade, much attention has been devoted to the Mg isotope geochemistry of carbonate for the potential to reconstruct seawater chemistry (Geske et al., 2012; Kasemann et al., 2014; Higgins and Schrag, 2015; Hu et al., 2017; Mavromatis et al., 2017; Hu et al., 2021a, 2021b, 2022b; Zhang et al., 2022). Interpreting Mg isotopes of calcite or marine limestones has been significantly challenged by the post-depositional alteration (Riechelmann et al., 2016; Hu et al., 2017; Ma et al., 2018b) and the complicated Mg isotope fractionation associated with the crystallization paths (Chen et al., 2020; Li et al.,

2012; Mavromatis et al., 2013; Mavromatis et al., 2017). Instead, Mg isotopes of dolomites have been widely used to trace changes of seawater chemistry, such as the Cenozoic seawater conundrum (Hu et al., 2022b), the restriction event in Paleotethys at the end-Permian (Hu et al., 2021b), the change of seawater Mg/Ca ratios at late Ediacaran (Zhang et al., 2022) and deglaciation at the end-Cryogenian (Kasemann et al., 2014; Liu et al., 2014).

It should be noted that Mg isotope compositions of dolomites are principally controlled by the porewater chemistry during the dolomitization process and hydrological conditions in dolomitization systems, as manifested by the concepts of “seawater-buffered” condition and “sediments-buffered” condition (Ahm et al., 2018; Higgins et al., 2018). In the “sediments-buffered” condition, the diffusion of dolomitization fluid can cause enigmatic changes of $\delta^{26}\text{Mg}$ in dolomites due to the evolution of pore-water chemistry (Fantle and Higgins, 2014; Blättler et al., 2015; Ahm et al., 2018; Higgins et al., 2018). Therefore, previous relevant studies emphasized the importance of the massive

* Corresponding author.

E-mail address: zhongyahu@tongji.edu.cn (Z. Hu).

dolostone sequences (Hu et al., 2017, 2019; Li et al., 2019; Hu et al., 2021a), which are supposed to form in the “fluid-buffered” condition (Hu et al., 2019). However, it is essential to recognize that the massive dolostone successions in geological history perhaps formed via the stacking of a multistage of dolomitization events (Lumsden and Caudle, 2001; Meister et al., 2013). The study by Ning et al. (2020) has shown that the stacking of multistage dolomitization events in the tidal plat environment, which are linked to sea-level fluctuation, can lead to various stratigraphic cycles of $\delta^{26}\text{Mg}$ values in a completely dolomitized carbonate profile. A recent study suggested that the fluid flow event on a basin scale during deep burial stage can also cause the created gradients in Mg isotope compositions of dolomite bodies (Kimmig et al., 2021). More investigation on the Mg isotopic variability of dolomites in different sedimentary environments will be desirable for distinguishing changes of seawater chemistry and dolomitization effects, which is the key for the reconstruction of seawater Mg isotopes.

Previous studies have well constrained the sedimentary background, including the sea level changes, geological ages, and tectonic evolution, for the deposition of massive dolostone in the Quse Formation of the lower Jurassic in the northern Tibet (Han et al., 2016; Ma et al., 2017). In this work, we performed a high-resolution, multi-proxy study of the dolostone succession in Quse Formation of the lower Jurassic in the Qiangtang Basin. To constrain the changes of seawater chemistry and dolomitization processes, we study the Mg–Sr–C–O isotope systematics, major and trace element concentrations, as well as petrographic and mineralogical features of the carbonate rocks. The change of geochemical compositions in the profile is generally characterized by the co-variation between Mg–C isotopes and trace element contents. The aims of this study include 1) to explore the response of Mg–C isotope and trace element in dolomite to the sea-level fluctuation, 2) to integrate multiple isotopic

and elemental proxies to distinguish records between environment changes and early diageneses for better interpreting Mg isotopes of dolomites; and 3) to quantify the stratigraphic evolution of dolomite $\delta^{26}\text{Mg}$ values when the hydrological system varied between “fluid-buffered” condition and “sediment-buffered” condition.

2. Geological setting

The studied section is located in the south Qiangtang Basin in the northern Tibetan Plateau (Fig. 1A), with an altitude of ca. 4600 m. The Qiangtang Basin covers $18.5 \times 10^4 \text{ km}^2$ in the central part of the Tibetan Plateau (Fu et al., 2010; Xue et al., 2020). The northern and southern boundaries of the basin are the Hol Xil–Jinsha River suture and Bangong Lake–Nujiang suture zone, respectively (Ma et al., 2017, 2018a; Xue et al., 2020). The Qiangtang basin is subdivided into northern Qiangtang and southern Qiangtang basins by the Central Uplift (Wang et al., 2008; Fu et al., 2016b; Ma et al., 2018a). During Late Triassic to Middle Jurassic, the south Qiangtang Basin as a part of the eastern Tethyan domain underwent long-term stable subsidence, and marine sediments were widely deposited on the continental margin of Bangong–Nujiang ocean in the northeastern Tethys (Ma et al., 2017; Hu et al., 2022a).

The Mesozoic strata in the southern Qiangtang Basin are over 4000 m and are dominated by the Jurassic sequences (Fig. 1B). The upper Triassic strata are composed of shallow marine sandstones, mudstones, and limestones (Fig. 1B). During the Early Jurassic, the Quse and Sewa formations were deposited in the basin. The Quse Formation in the study area is ascribed to shallow-marine facies, consisting of limestones and dolostones (Fig. 1B and C) (Ma et al., 2017), while some studies ascribed the black shale, marl, and mudstone resembling that of the Sewa Formation to the upper Quse Formation (Fu et al., 2016a). Until the

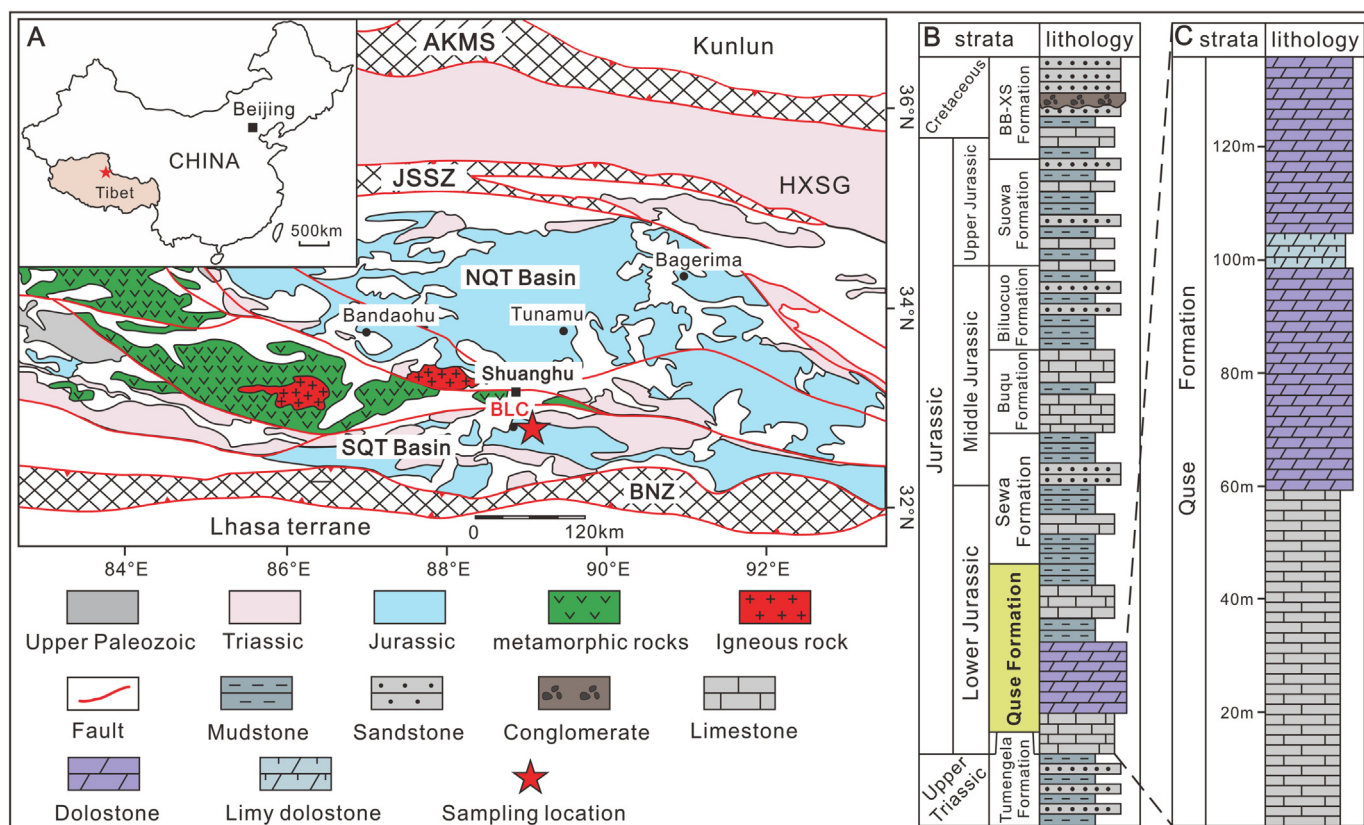


Fig. 1. Geological map showing sampling site in Tibet and the Mesozoic stratigraphy in the study area. (A) Map showing the location of the field section, AKMS–Ayimaqin–Kunlun Mutztagh suture, HXSG–Hoh Xili–Songpan Ganzi, JSSZ–Jinshajiang suture zone, NQT Basin–North Qiangtang Basin, SQT Basin–South Qiangtang Basin, BNZ–Bangong–Nujiang suture zone (modified from Xue et al., 2020); (B) the Mesozoic stratigraphic features in the research area (based on Fu et al., 2016b and Ma et al., 2018a), BB-XS formation refers to the Bailong Binghe and Xueshan Formations; (C) detailed stratigraphic feature of the lower to middle part in the Quse Formation of the Biluoctuo section, based on field observation.

Middle Jurassic, the southern Qiangtang Basin has transformed into a broad carbonate platform in the context of ongoing transgression (Fu et al., 2016b; Hu et al., 2022a). The Buqu Formation which was deposited at this stage mainly consisted of bioclastic limestones, and dolostones (Fig. 1B). A widespread regression occurred since the late Middle Jurassic (Callovian stage), and deposited Biluocuo and Xiali formations, which consist of sedimentary clastic rocks with carbonates interlayers (Fig. 1B). The Suowa Formation, which was deposited during the Late Jurassic is a transgression sequence, consisting of limestones, and marls and shales (Fig. 1B) (Fu et al., 2016b; Ma et al., 2017; Hu et al., 2022a).

The outcrop in this study is located on the east side of Biluo Co (BLC) ($32^{\circ}53'17''N, 88^{\circ}52'57''E$), approximately 50 km to the south of Shuanghu County (the red star in Fig. 1A). The road construction well exposed the carbonates of the Quse Formation (Fig. 2A), which were deposited at the Pliensbachian to Toarcian stages according to the newly reported ammonite fossils (Ma et al., 2017). In the BLC section, the exposed Quse Formation in the section is about 135 m in thickness, two sub-units can be divided for the Quse Formation (Fig. 1C). The lower part consists of pure limestones, from 0 m to 60 m, 60 m thick in total, and the upper part is dominated by dolostones, from 60 m to 135 m, 75 m thick in total (Fig. 1C). The dolostone succession abruptly overlay on the limestone

interval without the gradual transition (Fig. 1C). On the profile, the thickness of each single carbonate layer is 20 cm to 40 cm (Fig. 1A). During the field work, no hydrothermal veins (like quartz and calcite veins) or faults were observed in this carbonate profile. The dolostones are generally gray-to white-colored in the outcrop, and the reddish soil overlying the outcrop dyed the surface of rocks (Fig. 2A, B). The underlain limestone succession consists of the grayish, horizontally bedded layers (Figs. 1C, 2A).

3. Sampling and methods

The sampling of the carbonate in Quse Formation was performed in the summer of 2020. The carbonates in the section were sampled nearly every 1 m except for some intervals which were covered by Quaternary deposits. In the lithological transition interval, we increased the sampling density. Totally one hundred and thirty-four carbonate samples were collected. The sampled rocks are fresh and devoid of any sign of surface weathering.

In the laboratory, one hundred and twenty-four carbonate samples were made into rock slices for observing the petrological and mineralogical features, as well as powdered for X-ray diffraction analyses. We totally made 124 thin sections from these 124 rock slices. According to

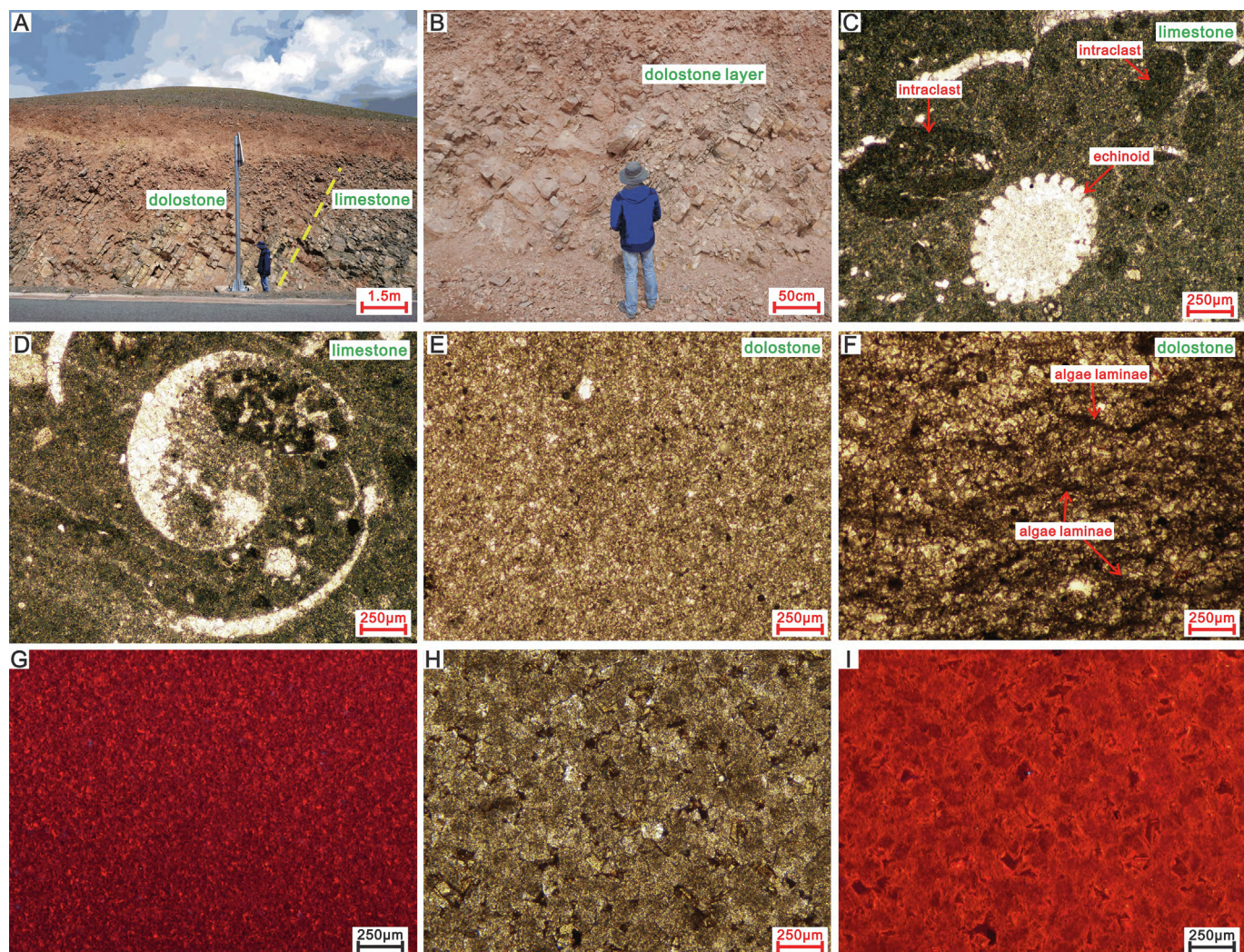


Fig. 2. Photographs showing the petrographic characteristics of the Quse Formation in the Biluocuo section. (A) Cross-section of the Biluocuo section, the dashed yellow line is the boundary between limestone interval in the lower part and dolostone interval in the upper part, person for scale is ca. 1.7 m tall; (B) the tabular cross-bedded dolostone layers in the outcrop; (C) the wackestone in the limestone interval, containing echinoid fossil and intraclasts, 21 m; (D) the well-preserved gastropod fossil in the wackestone, 51 m; (E) the dolomiticrite in the dolostone interval, 65 m; (F) fine-crystalline dolostones with algae laminae, 105 m; (G) the CL photograph showing the crystal features of dolomites in (E); (H) the features of coarse-grained dolomites which we did not select for geochemistry analyses; (I) the CL photograph showing the crystal features of dolomites in (H).

the lithological and mineralogical changes, to avoid the effects of hydrothermal alteration or multiple dolomitization processes, we did not select the dolostones which are composed by coarse-crystal dolomites for geochemistry analyses. Totally, forty-five carbonate samples were selected for trace element analyses, and thirty-nine dolostone samples among them were selected for Mg isotope analyses. Then, according to the variation of petrological features, as well as trace elemental and Mg isotope compositions along the profile, we selected twenty-eight samples for C—O isotopic analyses. Due to the invariability of trace elements and $\delta^{13}\text{C}$ - $\delta^{18}\text{O}$ values in limestone interval, we only selected twenty-five samples which are mostly from the dolostone interval for Sr isotope analyses.

3.1. Petrography and mineral analyses

Cathodoluminescence microscopy was performed on a cold-cathode instrument (type CL8200-MK5) with an acceleration voltage of 13–14 kV, a current of 250–300 mA, and a chamber pressure of 0.03–0.05 mBar (Hu et al., 2019). The bulk carbonate rocks were powdered into 300 mesh in the agate mortar. The XRD analyses for the bulk carbonate powder were performed on a Rigaku Rapid II dual-source X-ray Diffractometer, at Nanjing University. The instrument is equipped with an imaging plate, and a rotating anode Mo target ($\text{Mo K}\alpha = 0.714 \text{ \AA}$). 5 min exposure was set for each sample. The voltage and current were set as 50 kV and 90 mA, respectively. In this study, the mineralogical constitutions and abundance (dolomite vs calcite) in bulk carbonate rocks are estimated based on the intensities of 104 peaks as identified by MDI Jade 6.5 software.

3.2. Trace elemental analyses

Twenty mg powder of each sample was dissolved in 5 mL 15 % acetic acid on a hotplate at 95 °C for 24 h. Nitric acid and hydrochloric acid were not used during the digestion process to avoid the contamination of terrigenous silicate materials. 1 mL solution was transferred into a new precleaned Teflon beaker and repeatedly dried with 1 mL concentrated HNO_3 on a hotplate for three times to completely transform the sample into nitrate. Then, the dried sample was re-dissolved in 10 mL 2 % HNO_3 for trace elemental analyses. The measurement of trace element concentrations was performed on an Agilent 7900 ICP-MS at the State Key Laboratory of Marine Geology at Tongji University. The dolomite standard material (JD0-1) was dissolved and analyzed to monitor the geochemical treatment and data quality. The analytical precision was better than 5 % (RSD) for all selected elements.

3.3. Carbon ($\delta^{13}\text{C}$) and oxygen ($\delta^{18}\text{O}$) isotope analysis

Twenty-eight carbonate samples were selected for C—O isotopic analyses using a Thermo Finnigan Delta V Plus isotope ratio mass spectrometer (IRMS) at the State Key Laboratory for Minerals Deposit Research at Nanjing University. The procedures have been detailed documented by Li et al. (2019). In brief, 100 µg powders were weighed and reacted with 30 µL ~100 % phosphoric acid at 70 °C to fully transform the CO_3^{2-} into CO_2 for C—O analyses. The C—O isotope ratios of carbonates were normalized to the values of V-PDB standard and reported as per mil (‰). The analytical precision is better than 0.10 % and 0.05 % (standard deviation, 1SD) for $\delta^{13}\text{C}$ and $\delta^{18}\text{O}$, respectively.

3.4. Strontium ($^{87}\text{Sr}/^{86}\text{Sr}$) isotope analysis

Twenty-five samples which once had been analyzed C—O isotope compositions were selected for strontium isotope analysis. The procedure has been described by Su et al. (2021). The dissolved solution containing 2 mg Sr was extracted and dried. The sample was first transformed into nitrate, and then dissolved in 1 mL 3 N HNO_3 for ion exchange chromatography. Strontium isotope ratios of these carbonate samples

were measured using a Thermo Fisher Scientific Neptune Plus MC-ICP-MS at Tongji University. USGS rock standards (AGV-2 and BCR-2) were processed along with the samples. The measured $^{87}\text{Sr}/^{86}\text{Sr}$ ratios of AGV-2 and BCR-2 were 0.7039690 ± 0.000007 (2σ , $n = 2$) and 0.705033 ± 0.000007 (2σ , $n = 4$), respectively, being consistent with the published values (Raczeck et al., 2003). Repeated analyses of pure Sr solution NBS987 yielded $^{87}\text{Sr}/^{86}\text{Sr} = 0.710267 \pm 0.000008$ (2σ , $n = 13$).

3.5. Magnesium isotope ($\delta^{26}\text{Mg}$) analysis

Based on the XRD analyses, thirty-nine dolostone samples (dolomite >70 wt%) were selected for Mg isotope analyses. We extracted an aliquot of the stock solution that contained 50 µg Mg, and treated with 0.5 mL concentrated nitric acid and evaporated on a plate at 95 °C for three times to convert salts to nitrate form. The ion exchange procedures we employed in this study to purify Mg from the samples have been described by Hu et al. (2017, 2023) in detail. After the treatments, matrix elements were <0.2 % in the pure Mg solution and the recovery was >98 %.

The analyses of magnesium isotope ratios were performed on a Thermo Fisher Scientific Neptune Plus MC-ICP-MS at Nanjing University. The instrument was running at low-mass-resolution mode, using a 100 µL/min self-aspirating nebulizer tip and a glass spray chamber. The Mg concentrations of all samples and standards are 500 ppb. The typical internal precision (2 standard error or 2 SE) was better than ± 0.04 % for $^{26}\text{Mg}/^{24}\text{Mg}$ and ± 0.02 % for $^{25}\text{Mg}/^{24}\text{Mg}$. The pure Mg solutions of Cambridge 1 and DSM 3 were also analyzed to monitor the analytical accuracy of Mg isotopic ratios (Supporting Material Table S1). To monitor our chemical purification method, IAPSO seawater standard and USGS rock reference materials (BIR-1a and DTS-2b) were processed in the ion exchange procedure. The $\delta^{26}\text{Mg}$ values of the standard samples in our study well match the reported values in literature (within ± 0.05 %, Supporting Material Table S1). All measured data were normalized to the international Mg isotope standard (DSM 3) using the conventional δ notation to express per thousand deviations.

4. Results

4.1. Petrography and mineralogy

Most carbonate rocks in the limestone interval are the micritic limestone, no recrystallization and overgrowth of the calcite were observed (Fig. 2C, D). The gastropod and echinoid are the major biota, and can be identified in the micritic matrix (Fig. 2C, D). Biological fossils are generally rare in most carbonate rocks. Totally, only four samples can be identified as wackestone. The diameters of these fossils commonly range from 250 µm to 500 µm (Fig. 2C, D). As indicated by the bulk-rock XRD analyses, the calcite contents of the micritic limestones are >97 % and almost all these limestone samples contain minor quartz, ranging from 1 % to 3 % (Fig. 3).

No biological fossils were observed in the dolostones. Dolomite contents in the dolostone interval are mostly >95 %, without regular stratigraphic variability (Fig. 3). In this study, the dolostones are mostly composed by the fine-grained subhedral to anhedral dolomites (<50 µm) (Fig. 2E, F). These dolomites display the dull red luminescence, and lack of the hydrothermal alteration and overgrowth (Fig. 2E–G). The coarse-crystal dolomites (Fig. 2H) also exhibit the dull red luminescence without the typical zones or rims under CL (Fig. 2I). In the top 20 m of the profile, several dolostone samples contain algal lamination with slightly coarse crystal sizes (Fig. 2F). According to XRD analyses, no systematic changes in the dolomite crystal lattices were detected. The d_{104} values of the dolomites in our selected dolostone samples range from 2.893 to 2.906 without the stratigraphic changes along the profile (Supporting Material Table S2). According to the empirical curve proposed by Zhang et al. (2010), the calculated MgCO_3 contents in the dolomite crystals are ~46–49 mol%.

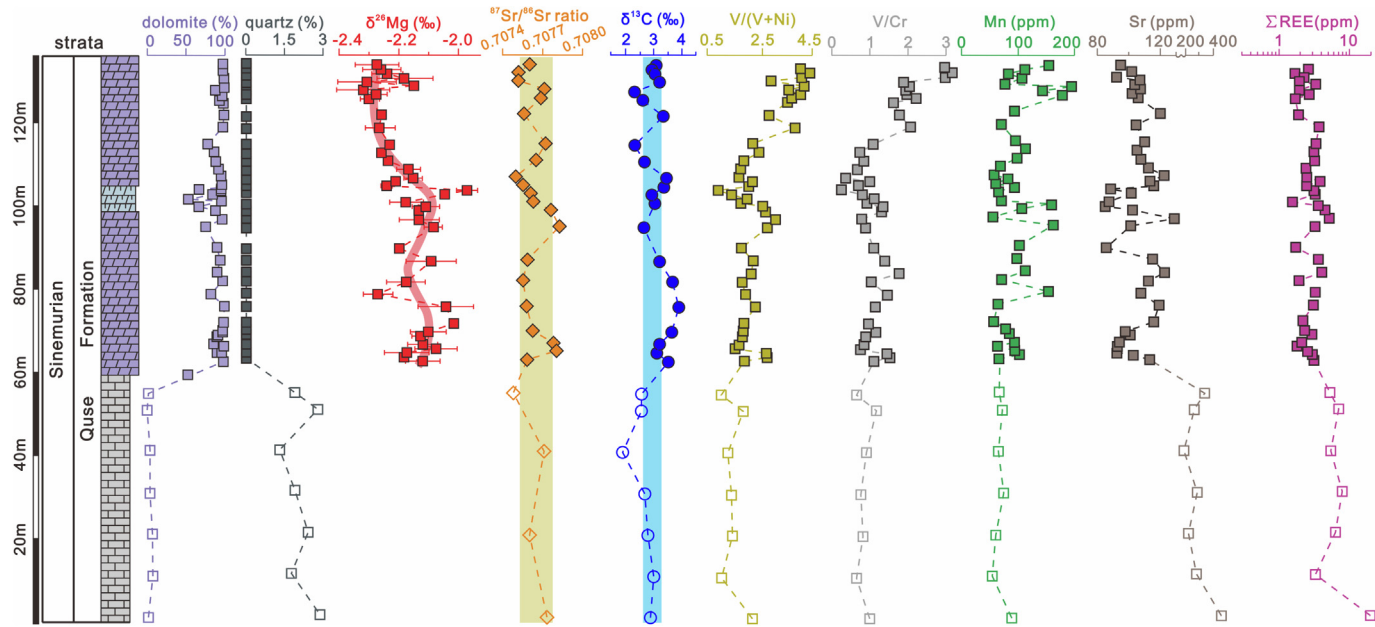


Fig. 3. Lithologic column showing variations in mineral components, trace elemental compositions and Mg-C-Sr isotopic compositions. The open and filled shapes represent the data of limestone and dolostones, respectively. The yellow and blue bars refer to the $^{87}\text{Sr}/^{86}\text{Sr}$ ratios and $\delta^{13}\text{C}$ values of the Early Jurassic seawater, and the data are from Veizer et al. (1999).

4.2. Trace elements

Rare earth elements (REEs) in limestones vary from 3 to 19 ppm, while dolostones of the Quse Formation have slightly lower REE contents, ranging from 1 to 4 ppm (Fig. 3). The average Zn content in limestone and dolostone is ca. 5 ppm and 66 ppm, respectively (Supporting Material Fig. S3). Vanadium (V), nickel (Ni) and chromium (Cr) contents in the bulk carbonates are 2–10 ppm, 9–28 ppm, and 3–10 ppm, respectively (Supporting Material Fig. S3). Along the outcrop, the V/(V + Ni) and V/Cr ratios of carbonates maintain stable in the limestone interval and lower part in the dolostone interval (0 m to 80 m), whereas in the upper dolostone succession (ca. 80 m to 140 m), the V/(V + Ni) and V/Cr ratios consistently increase upward (Fig. 3). Titanium (Ti) content of carbonates in the Quse Formation mostly ranges from 2 to 10 ppm (Fig. 4A). The V/Cr and V/(V + Ni) ratios in the carbonates lack a correlation with Ti contents (Fig. 4A, B). Manganese contents in the limestone range from 50 to 87 ppm, while the dolostones in the upper section have relatively high Mn contents, ranging from 80 to 200 ppm (Fig. 3). Strontium contents in the limestones range from 170 to 450 ppm, and across the lithological boundary in the profile, the Sr contents decreased rapidly to <120 ppm in the upper dolostone unit (Fig. 3).

4.3. Isotope geochemistry

The $\delta^{13}\text{C}$ and $\delta^{18}\text{O}$ values of carbonates in the Quse Formation range from 2 ‰ to 4 ‰ and −9 ‰ to −1 ‰, respectively (Fig. 4C). The carbonate $\delta^{13}\text{C}$ values lack the correlation with $\delta^{18}\text{O}$ values (Fig. 4C). The bulk-rock $\delta^{13}\text{C}$ values did not display co-variation with V/Cr or V/(V + Ni) ratios (Fig. 4D, E), however, in dolostones, $\delta^{13}\text{C}$ values exhibited a negative correlation with Mn contents (Fig. 4F).

$^{87}\text{Sr}/^{86}\text{Sr}$ ratios of carbonate in the BLC section mostly range from 0.70755 to 0.70775 (Fig. 3). The bulk-rock $^{87}\text{Sr}/^{86}\text{Sr}$ ratios did not exhibit any correlation with Ti, Rb, or Sr contents (Supporting Material Fig. S1).

The $\delta^{26}\text{Mg}$ values of dolostones range from −2.32 ‰ to −1.97 ‰, with an average value of -2.18 ± 0.18 ‰ (2SD, $n = 39$; Fig. 3). The bulk-rock $\delta^{26}\text{Mg}$ values do not show a correlation with Ti contents (Fig. 5A) or dolomite contents in the bulk carbonates (Supporting Material Fig. S2C). Overall, $\delta^{26}\text{Mg}$ values in the dolostone layers decrease upward

from ca. −2.1 ‰ to ca. −2.3 ‰ (Fig. 3). In the section, the upward decrease in $\delta^{26}\text{Mg}$ is mirrored by the increase in V/Cr, V/(V + Ni) ratios, and Mn contents (Fig. 3). As a result, $\delta^{26}\text{Mg}$ values generally negatively correlate with these trace elemental proxies (Fig. 5B–E). $\delta^{26}\text{Mg}$ values of dolomites have a slight positive correlation with $\delta^{13}\text{C}$ values (Fig. 5F).

5. Discussion

5.1. The negligible effects of deep-burial diagenesis alteration

The micritic structure of the limestones (Fig. 2C, D) and dull red luminescence of dolomites (Fig. 2E–G) demonstrated the insignificant post-deposition alteration on mineralogical features. $\delta^{13}\text{C}$ values and $^{87}\text{Sr}/^{86}\text{Sr}$ ratios are both well comparable to the values of coeval seawater (Fig. 3). In addition, the Mn/Sr ratios and $\delta^{18}\text{O}$ values of most carbonates are lower than 2 (Fig. 5E) and higher than −5 ‰ (Fig. 4C), respectively. As such, these geochemistry signals are consistently indicative of negligible high-temperature reworking (Kaufman et al., 1993; Swart, 2015; Immenhauser, 2022). On the other hand, in the massive dolostone sequences, Mg isotopes of dolostone are commonly robust against diagenetic processes (Geske et al., 2012; Hu et al., 2017, 2019; Qing et al., 2023). Even when dolomite crystal morphology was modified by diagenesis or hydrothermal alteration, $\delta^{26}\text{Mg}$ values can remain invariable (Hu et al., 2019; Ning et al., 2019; Qing et al., 2023). Therefore, multiple lines of evidence suggest that the Mg-C-O-Sr isotopic and elemental compositions of the carbonates in the BLC section are well preserved since the deposition.

5.2. The sea-level changes recorded in carbonates

Since the end of the Triassic, the global sea level underwent a long-term rise and peaked at the early Toarcian of the Early Jurassic (Hallam, 2001; Miller et al., 2005). In Tibet, the eustatic sea level changes during the Early to Middle Jurassic were represented by three stepwise transgressions (Han et al., 2016). The deposition of the Quse Formation witnesses the long-term rise of sea level (Han et al., 2016; Ma et al., 2017) (Fig. 6). In the BLC section, the eustatic sea-level changes have been recorded by the stratigraphic changes of mineral compositions, lithological features, and trace elemental proxies in carbonates.

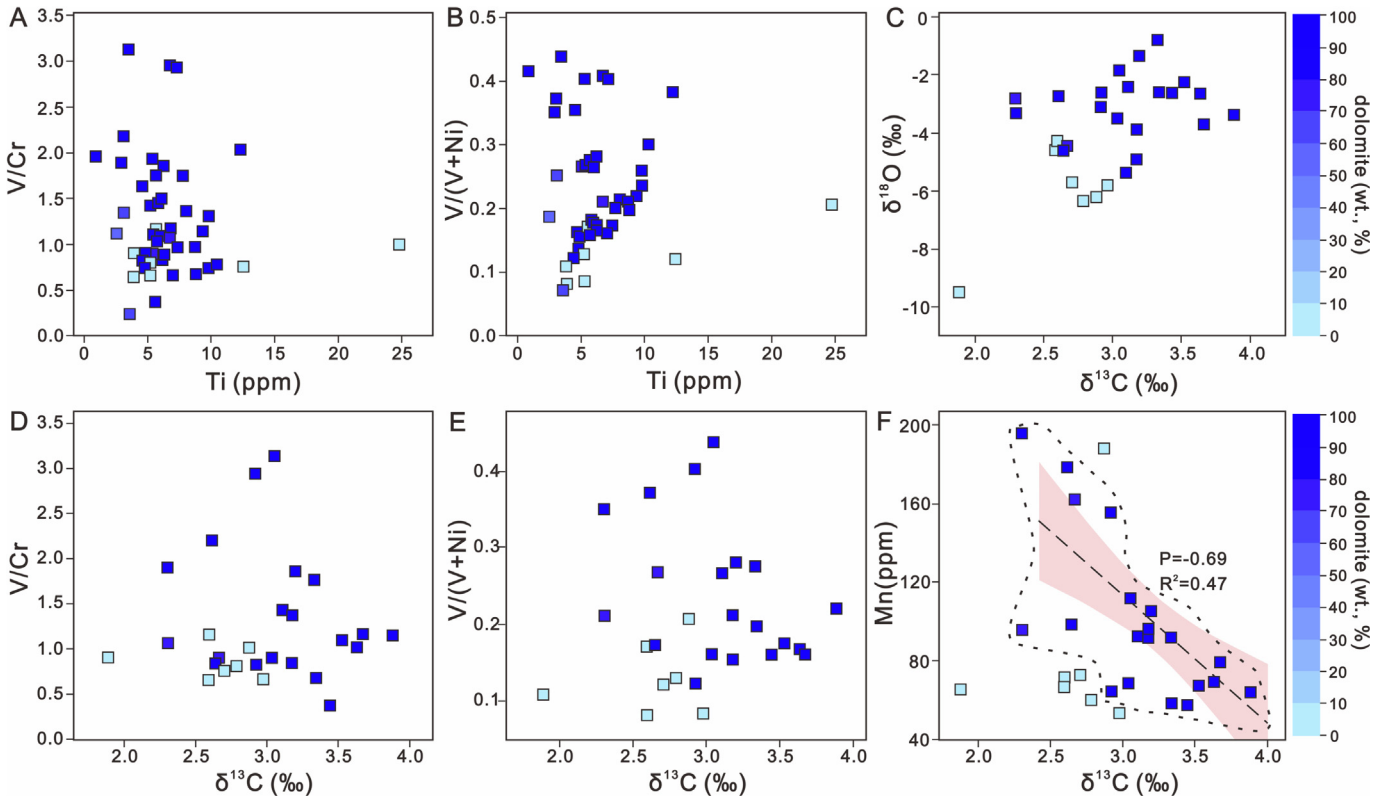


Fig. 4. Cross-plots of trace element contents and C–O isotope compositions. The change of the color in each figure refers to the variation of dolomite contents in the bulk carbonate. (A) V/Cr ratios versus Ti contents; (B) V/(V + Ni) ratios versus Ti contents; (C) $\delta^{13}\text{C}$ values versus $\delta^{18}\text{O}$ values; (D) V/Cr ratios versus $\delta^{13}\text{C}$ values; (E) V/(V + Ni) ratios versus $\delta^{13}\text{C}$ values; (F) Mn contents versus $\delta^{13}\text{C}$ values, the linear fitting curve shows the correlation between Mn contents and $\delta^{13}\text{C}$ values in the dolostones (including the data points in the dash-line box).

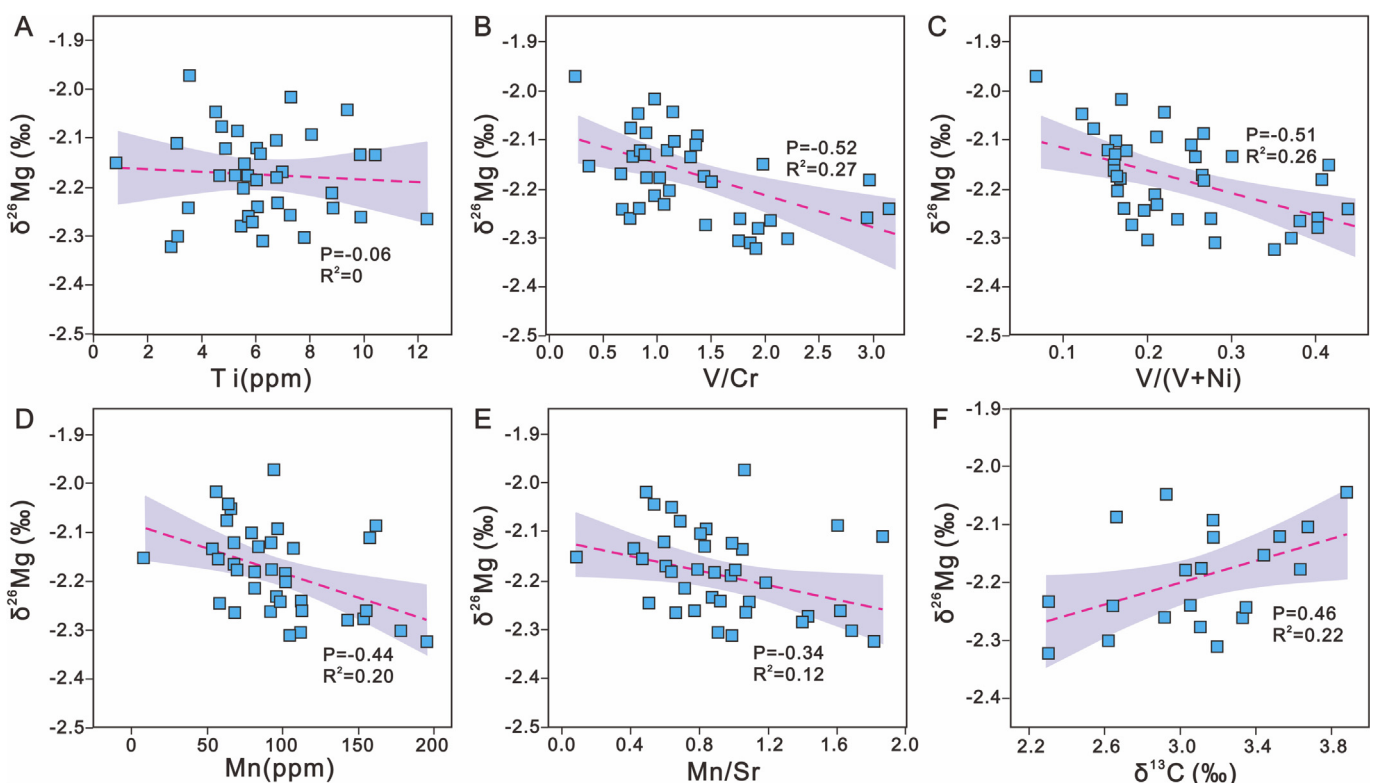


Fig. 5. Cross-plots showing the variation of Mg isotope compositions in dolostones. (A) Ti contents versus $\delta^{26}\text{Mg}$ values; (B) V/Cr ratios versus $\delta^{26}\text{Mg}$ values; (C) V/(V + Ni) ratios versus $\delta^{26}\text{Mg}$ values; (D) Mn contents versus $\delta^{26}\text{Mg}$ values; (E) Mn/Sr ratios versus $\delta^{26}\text{Mg}$ values; (F) $\delta^{13}\text{C}$ values versus $\delta^{26}\text{Mg}$ values.

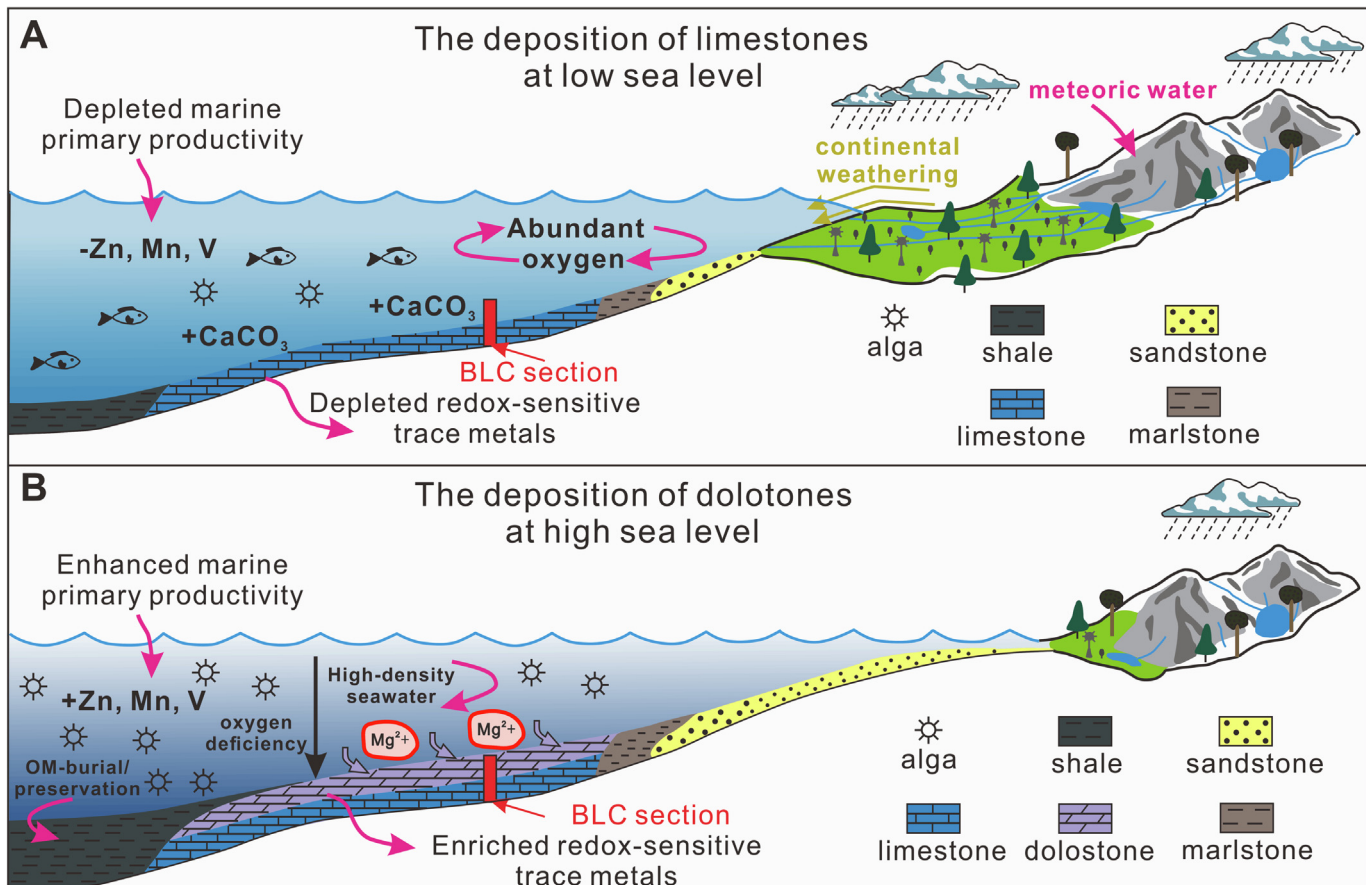


Fig. 6. The conceptual model showing the eustatic sea level changes, the sedimentary evolution and the variation of seawater chemistry during the formation of carbonate in the Quse Formation.

The slightly high REE and quartz contents of the limestone in the lower part of the Quse Formation (Fig. 3) reflect a high continental runoff into the carbonate platform. The relatively high influx of freshwater into the platform probably diluted the seawater in the basin and hindered the dolomitization, accounting for the formation of thick limestone succession in the lower part of the Quse Formation (Fig. 6A). Thus, during the deposition of limestones in the lower Quse Formation, the carbonate platform is supposed to be the low sea-level stage with relatively high influx of continental runoff. The upward increase of V/(V + Ni) and V/Cr ratios indicates that the platform gradually evolved from an oxidic condition to a dysoxic condition (Hatch and Leventhal, 1992; Jones and Manning, 1994; Bennett and Canfield, 2020). From the Jurassic to the late Cretaceous, the rapid rise of sea levels tightly related to several large-scale anoxic events in the bottom water (Wang et al., 2014; Han et al., 2016, 2018; Hu et al., 2020). The rise of sea level will lead to the expansion of the carbonate platform (Shao et al., 2017; Hu et al., 2022b). Such an expanded platform could largely buffer the dilution effect of freshwater influx, and the evaporation in a larger platform can lead to the increase of seawater salinity and produce more dolomitization fluid accounting for the pervasive dolomitization (Machel and Mountjoy, 1986; Budd, 1997) (Fig. 6B). Notably, dolostones from the upper Quse Formation contain elevated Mn concentrations (Fig. 3) that negatively correlate with δ¹³C values (Fig. 4F), which most likely reflected the degradation of organic matters and the Mn (IV) reduction reaction (i.e., CH₃COO⁻ + 4MnO₂ + 3H₂O → 4Mn²⁺ + 2HCO₃⁻ + 7OH⁻) (Burdige, 1993; Petrush et al., 2015 and 2017; Li et al., 2019). This process would result in the enrichment of Mn²⁺ in pore water and isotopically light carbon in the dissolved inorganic carbon (DIC). Thereby, the dolostones in the upper Quse Formation formed in the Mn (IV) reduction zone, where the bottom

water is suboxic or dysoxic, and microbial process in such condition promoted the dolomitization (Fig. 6B). We note that δ¹³C values of the carbonates overlap with the value of Early Jurassic seawater (δ¹³C ≈ 2.5‰–3.5‰; Veizer et al., 1999) (Fig. 3), and the variation is within 2.5‰. According to our observation during the field work, most carbonates display light gray to white color (Fig. 2), implying the low contents of organic matter in the sediments. Therefore, the Mn (IV) reduction intensity is not strong enough to completely reset the bulk-rock carbon isotope compositions.

5.3. Mg isotope systematics of dolostones in Quse Formation

The terrigenous detrital materials were not detected by petrographic observations and XRD analyses of the dolostones from the BLC section (Fig. 2E, F). The Ti contents of dolostone samples are mostly <10 ppm, and display no correlation with δ²⁶Mg values (Fig. 5A). Therefore, the contamination of Mg from terrigenous detritus on the bulk-rock Mg isotope compositions of carbonate is negligible. On the other hand, the dehydration of clay minerals in marlstones is incapable of providing enough Mg²⁺ for pervasive dolomitization (Li et al., 2016). The δ¹³C values and ⁸⁷Sr/⁸⁶Sr ratios of dolostones in the Quse Formation well match the values of coeval seawater, respectively (Fig. 3). Therefore, the coeval seawater was the dolomitization fluid, providing the sufficient Mg source for the formation of massive dolostones. Due to the lack of evaporites in the strata, including gypsum and halite, the dolomitization fluid is most likely the penesaline seawater, rather than hypersaline seawater (Qing et al., 2001). δ²⁶Mg values of bulk dolostones did not have any correlation with dolomite contents, *d*₁₀₄ values of dolomites, or other indexes of crystal lattices (Supporting Material Fig. S2), ruling out the influence of dolomite contents or lattice

parameters on Mg isotope compositions. Therefore, exploring the dolomitization processes and mechanism is the key to elucidate the Mg isotopic variability in dolostones.

There are two possible scenarios accounting for the formation of massive dolostone sequences in the Quse Formation: 1). the stacking of multistage dolomitization event caused by the periodic downward migration of dolomitization fluid at early diagenesis stage (Ning et al., 2020); 2). syn-depositional origin (Machel and Mountjoy, 1986; Hu et al., 2022b). Both dolomitization processes occurred at the early diagenesis stage. In the former scenario, the thick dolostone layers formed as the result of multiple downward migration of dolomitization fluid since the deposition of the whole limy sediment column. According to the observation of Cenozoic dolomitization case as revealed by IODP drill cores, such downward migration of dolomitization fluid can reach 400 m in depth (Blättler et al., 2015; Higgins et al., 2018). However, in the later scenario, the dolomitization process occurs very soon after the deposition of limy sediments before the deposition of subsequently dolomitized beds, dolomites formed at the seawater–sediment interface (Machel and Mountjoy, 1986).

During the downward migration of dolomitization fluid, due to the preferential uptake of ^{24}Mg by dolomite, dolostones that formed at the early stage in the upper part of the succession are always isotopically lighter than that formed in deeper sediments (Huang et al., 2015; Ning et al., 2020). This feature seems to resemble the stratigraphic variability as shown in Fig. 3. As the discussion above, the Mn (IV) reduction reaction was involved in the dolomitization processes. If the massive dolostones formed during the multistage downward migration of dolomitization fluid, when the dolomite with the highest Mn content at the top sediment column precipitated in the Mn (IV) reduction zone, the diagenesis systems below this layer are supposed to be in a more hypoxic condition (Petraš et al., 2015, 2017). However, on the contrary, as indicated by the redox-sensitive elemental proxies, including V/(V + Ni) and V/Cr, the sedimentary/early diagenetic systems in the sediment column became progressively oxidizing downwards (Fig. 3). In addition, the studies on modern/Cenozoic dolomitization cases in the IODP cores indicated that the early diagenetic systems in the iron oxide zone or sulfate reduction zone are mostly “sediment-buffered”, where the $\delta^{26}\text{Mg}$ values of dolomites can be highly variable, over 1 ‰, accompanying with significant depletion of ^{13}C (Blättler et al., 2015). By comparison, the dolostones in the lower part of dolostone sequences (from 60 m to 100 m in the sediment column) have homogeneous C and Mg isotope compositions (Fig. 3). Therefore, the trace elemental proxies, as well as C–Mg isotopic signals rule out the periodically long-distance downward migration of dolomitization fluid accounting for the formation of the tick dolostone layers of the Quse Formation.

Instead, we suggest a syn-depositional origin accounting for the formation of dolomite in the Quse Formation. The upward decrease of $\delta^{26}\text{Mg}$ values in dolomites most likely reflects the elevated marine connection between the platform/lagoon and the open ocean in the context of sea level rise. In brief, the preferential uptake of ^{24}Mg by dolomitization would lead to the enrichment of ^{26}Mg in the lagoon fluids, while the ongoing rise of sea level would lead to the replenishment of seawater from open ocean and then drift the Mg isotope composition of lagoon water toward the value of open ocean (Bialik et al., 2018; Hu et al., 2021a, 2021b), which is represented by the upward decrease of dolomite $\delta^{26}\text{Mg}$. Meanwhile, as the discussion in Section 5.2, the rise of sea level resulted into the dysoxic condition at the seafloor and facilitated the Mn (IV) reduction process in the sediments, as well as the decrease of $\delta^{13}\text{C}$ values of carbonates (Fig. 6B). According to previous studies, the Mn (IV) reduction can occur at the sites where are just tens of centimeters below the sediment–water interface (Burdige, 1993; Petraš et al., 2015, 2017). Therefore, the sediments were not tightly compacted, with high porosity and permeability. In such soft sediments, the dolomitization system has a high fluid/rock ratio for Mg but a lower fluid/rock ratio for C due to the high Mg:C ratio in seawater (for example $\text{Mg:HCO}_3^- = 27.5$ for modern seawater, Demicco

et al., 2005). As a result, Mg isotopes in dolomites were buffered by seawater, while carbon isotopes of DIC can be influenced by the decomposition of organic matter. In conclusion, the co-variation between Mg–C isotopes and trace elements recorded in the dolostone sequence from the BLC section in the Qiangtang basin reflected the changes of seawater chemistry caused by a rapid rise of sea level, rather than the diffusion process of porewater.

5.4. Insights into dolomite Mg isotopes for the reconstruction of seawater chemistry

5.4.1. A numerical modeling on the Mg isotopic variability during downward dolomitization events

The changes of hydrological conditions in dolomitization systems can exert significant influence on Mg isotope compositions of dolomite (Huang et al., 2015; Higgins et al., 2018; Fantle et al., 2020), and produce highly variable $\delta^{26}\text{Mg}_{\text{dol}}$ in the dolostone profiles (Ning et al., 2020). A single downward dolomitization event in a carbonate sequence, which was characterized by a dolomitization front, can be easily identified. The preferential uptake of ^{24}Mg by dolomite precipitation will lead to the enrichment of ^{26}Mg in subsequently precipitated dolomites in the profile (Huang et al., 2015), accompanying by the decline in dolomitization intensity due to the progressive decrease of Mg in the fluid.

We run dynamic numerical modeling to assess the coupling effect of multiple downward dolomitizations on $\delta^{26}\text{Mg}$ values in massive dolostone layers. In this model, we assume the eighty-meter dolostone strata as the stacking of 250-layer sediments (each layer is ca. 0.3 m, well matching the observation in field), and limy sediments in each layer are composed of 100-mole calcites. From the top to bottom in the profile, the original porosity in sediments before dolomitization was set to decrease from 90 % to 10 % considering the compaction effect. We assumed that during each downward dolomitization event, 4 mol calcites in the first-layer limy sediments will be dolomitized, and the fluid–mineral reaction rate decreased proportionally as the decline of porosity (Fig. 7A-1). The original Mg/Ca ratio and Mg concentration of dolomitization fluid are set as 10 and 100 mmol/kg, respectively. During dolomitization processes, the Mg in the solution will exchange with the Ca of the limy sediments and cause the drop of Mg/Ca ratio in the ambient fluid. The dolomitization unlikely occurs in the fluid with low Mg/Ca ratios, as a result, we assume the dolomitization would cease when the Mg/Ca ratio of pore water drops to 1 (Fig. 7A-2, the dashed blue line). During each dolomitization event, the $\delta^{26}\text{Mg}$ values of fluid ($\delta^{26}\text{Mg}_{\text{fluid}}$) and dolomites ($\delta^{26}\text{Mg}_{\text{dolo}}$) in each layer can be expressed as (n refers to the layer number):

$$\begin{aligned} &\delta^{26}\text{Mg}_{\text{fluid}(n+1)} \cdot \text{Mg}_{\text{fluid}(n+1)} + \delta^{26}\text{Mg}_{\text{dolo}(n)} \cdot \text{Mg}_{\text{dolo}(n)} \\ &= \delta^{26}\text{Mg}_{\text{fluid}(n)} \cdot \text{Mg}_{\text{fluid}(n)} \end{aligned} \quad (1)$$

$$\text{Mg}_{\text{fluid}(n+1)} + \text{Mg}_{\text{dolo}(n)} = \text{Mg}_{\text{fluid}(n)} \quad (2)$$

when the calcites in the layer were fully dolomitized by multiple dolomitization processes, the average $\delta^{26}\text{Mg}$ value ($\delta^{26}\text{Mg}_{\text{ave}}$) of dolomites in this layer is:

$$\delta^{26}\text{Mg}_{\text{ave}} \cdot \text{Mg} = \sum_{i=1}^m \delta^{26}\text{Mg}_i \cdot \text{Mg}_i \quad (3)$$

In Eq. (3), m represents the total number of dolomitization events, and $\delta^{26}\text{Mg}_i$ and Mg_i represent the $\delta^{26}\text{Mg}$ value and Mg content of the newly formed dolomites in each dolomitization event.

Modeling results indicated that $\delta^{26}\text{Mg}$ values of dolomites formed in the first dolomitization event display the ongoing downward rise as the evolution of pore-water chemistry (Fig. 7A-2, the dash dark yellow line), which is consistent with the literature (Huang et al., 2015). However, in the completely dolomitized profile, the variability of the average $\delta^{26}\text{Mg}$ value of dolomites ($\delta^{26}\text{Mg}_{\text{ave}}$) in different layers is represented

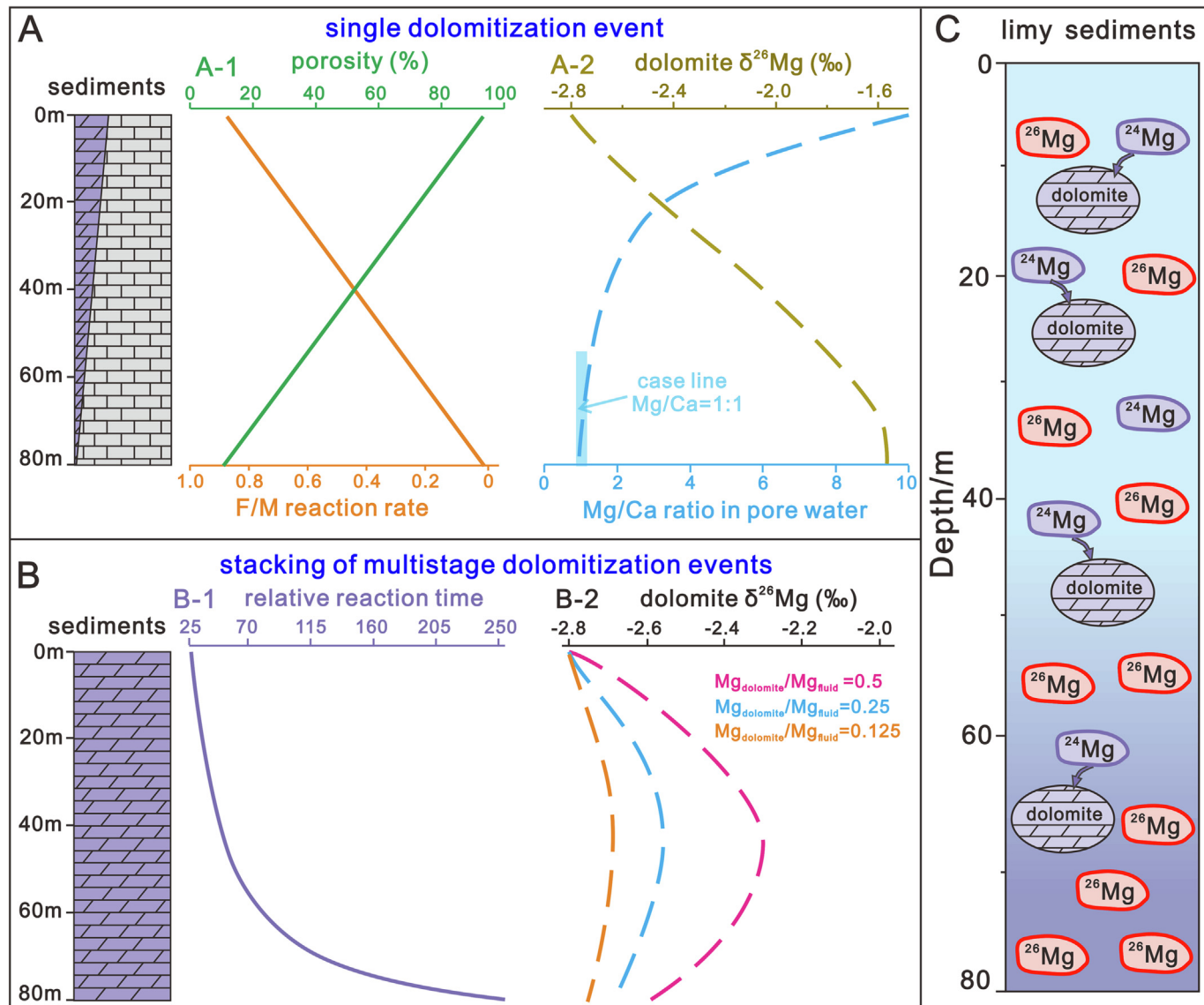


Fig. 7. The numerical modeling showing the variation of dolomite $\delta^{26}\text{Mg}$ during single downward dolomitization and stacking of multistage dolomitization events, respectively. The panel A-1 shows the original porosity in the limy sediments before dolomitization, F/M reaction rate refers to the fluid/mineral reaction rate, we assume that the reaction rate is highly depended on the porosity, the pale blue bar represents the case line of dolomitization when the Mg/Ca ratio of fluid was below 1. In panel B-1, the reaction time refers to the time which is needed for fully dolomitizing the limy sediment in the profile. In the designed model, we define the fluid/rock ratio as the ratio of total Mg content in fluid and Mg consumed by dolomitization in a single downward dolomitization event. Panel C shows the uptake of ^{24}Mg by dolomites and the enrichment of ^{26}Mg in the ambient fluid during the downward dolomitization.

by the downward enrichment of ^{26}Mg in the upper 40-meter interval and then shifts back to the values of dolomites in the first layer (Fig. 7B-2). Such a “boomerang” pattern in $\delta^{26}\text{Mg}$ ratio variability in the dolostone profile (Fig. 7B-2) is caused by the changes in the dolomitization rate and the time for the complete dolomitization in different layers. Specifically, due to the low porosity and fluid-sediment reaction rate in the lower sequences, when the sediments in the upper intervals have been completely dolomitized, the layers in the lower succession still contain large amounts of limy deposits (Fig. 7B-1). The Mg isotope compositions of fluid during the downward migration in the completely dolomitized layers are supposed to be unaltered, which is equal to the value of seawater. Then, in the lower units, Mg isotope compositions of dolomites precipitated from the unaltered dolomitization fluid are supposed to be equilibrium with coeval seawater, and thus the average $\delta^{26}\text{Mg}_{\text{dolo}}$ of dolomites in this layer would shift toward the value of dolomites precipitated from original dolomitization fluid.

Our result shows that the fluctuation amplitude of the dolomite $\delta^{26}\text{Mg}$ value is highly dependent on the flow rate of dolomitization fluid or the residual time of dolomitization fluid in the system

(Fig. 7B-2). In this model, we use the ratio of Mg consumed by dolomitization to total Mg mole amount in the fluid during each downward dolomitization to represent the flow rate of dolomitization fluid ($\text{Mg}_{\text{dolomite}}/\text{Mg}_{\text{fluid}}$). The $\text{Mg}_{\text{dolomite}}/\text{Mg}_{\text{fluid}}$ ratio was set as 0.5, 0.25 and 0.125, respectively. Our modeling result indicated that when the $\text{Mg}_{\text{dolomite}}/\text{Mg}_{\text{fluid}}$ ratio was 0.25 or even lower, the variation of $\delta^{26}\text{Mg}_{\text{dol}}$ along the completely dolomitized profile is within 0.2 ‰ (Fig. 7B-2). By a comparison, in natural marine condition, the water-sediment ratio for the pervasive dolomitization commonly far exceeded the maximum value in the modeling, mostly >300 (Wilson et al., 1990; Qing and Mountjoy, 1994), implying the extremely low $\text{Mg}_{\text{dolomite}}/\text{Mg}_{\text{fluid}}$ ratio and a much smaller variation of $\delta^{26}\text{Mg}_{\text{dol}}$ in the completely dolomitized carbonate profile than our modeling output. This inference is consistent with geological observed results, which show that $\delta^{26}\text{Mg}$ values in a dolostone sequence generated by stacking of multiple episodes of dolomitization events mostly varied within 0.2 ‰ (Ning et al., 2019, 2020). We proposed that the coupling effects of multiple dolomitization processes are prone to homogenize the Mg isotope compositions along the dolostone sequence.

As the insight shed by the modeling results, Mg isotopic variability of dolomites in the profiles has multiple explanations. Therefore, a comprehensive investigation on Mg—C isotopic and trace elemental proxies can provide better constraints for using Mg isotopes of dolomites to reconstruct the seawater chemistry. Through a comparison, previous work mostly focuses the attention on Mg isotopic variability in the dolostone layers within 10 m (Ning et al., 2020), which deposited in the tidal flat environments. Our modeling results mostly reflected integrated Mg isotope variability of dolomites in the huge-thick dolostone profile (nearly 80 m). On the other hand, our work quantified the stratigraphic changes of dolomite Mg isotopes when the flow rate of dolomitization fluid changed.

5.4.2. $\delta^{26}\text{Mg}$ values of Early Jurassic seawater in the eastern Tethys

Given that the dolomitization process can potentially modify the geochemistry of ambient fluid, leading to the rise of $\delta^{26}\text{Mg}$ values, we

ascrbe the lowest $\delta^{26}\text{Mg}$ of dolomites as being in equilibrium with the value of coeval seawater in the open ocean (north-eastern Tethys). Assuming the $\Delta^{26}\text{Mg}_{\text{dol}-\text{seawater}}$ fractionation factor of -2.0‰ for the dolomitization at early stage (Higgins and Schrag, 2010; Fante and Higgins, 2014; Li et al., 2015), $\delta^{26}\text{Mg}$ value of the Early Jurassic seawater as inferred from the records in Quse Formation is ca. -0.3‰ (Fig. 8). This value is significantly lower than the modeled $\delta^{26}\text{Mg}$ for Jurassic seawater by Li et al. (2015) (Fig. 8). Note that based on the data reported by Geske et al. (2012), the reconstructed seawater $\delta^{26}\text{Mg}$ value at the Norian (ca. 227 Myr) of the late Triassic is also lower than the predicted seawater $\delta^{26}\text{Mg}$ curve (Fig. 8). The only consistency is that the measured results and modeling prediction both display a long-term decrease of seawater $\delta^{26}\text{Mg}$ values from the Middle Anisian to the Jurassic (Fig. 8), which reflected the decrease of dolomitization intensity on a global scale (Wilkinson and Algeo, 1989; Li et al., 2015). Li et al. (2015) predicted the seawater $\delta^{26}\text{Mg}$ curve based

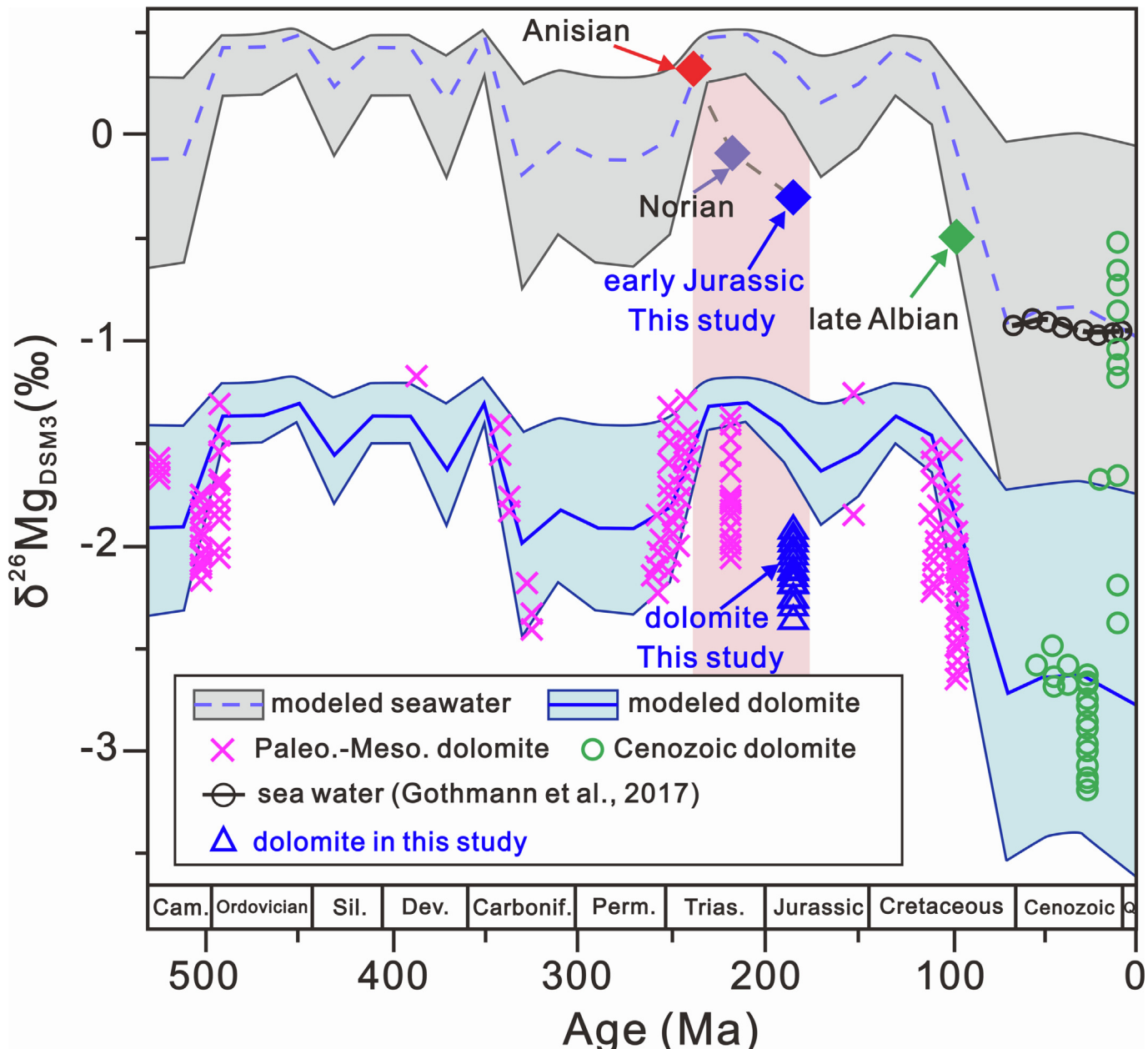


Fig. 8. $\delta^{26}\text{Mg}$ values of dolomite in the Phanerozoic and corresponding modeling results of Li et al. (2015). The data of measured $\delta^{26}\text{Mg}$ values of dolomites are cited from Jacobson et al. (2010), Geske et al. (2012), Azmy et al. (2013), Fante and Higgins (2014), Geske et al. (2015a, 2015b), Peng et al. (2016), Hu et al. (2017), Higgins et al. (2018), Bialik et al. (2018) and Hu et al. (2019, 2021a, 2021b). The $\delta^{26}\text{Mg}$ values of Cenozoic seawater are from Gothmann et al. (2017).

on a static Mg isotope mass balance model with the intensity of dolomitization in geological history as the input parameter. The discrepancy between the measured values in this study and the modeling prediction of Li et al. (2015) could indicate that the Mg influx in dolomitization from the Middle Triassic to the Jurassic was overestimated, although the long-term decline of dolomitization intensity, as traced by the seawater $\delta^{26}\text{Mg}$, probably holds the truth.

Since the Early Triassic, the carbonate productivity from Late Triassic to Early Jurassic decreased significantly, particularly at the Carnian of Late Triassic (ca. 237 Ma) (Sun et al., 2016; Jin et al., 2018), the end Triassic (Kiesling and Simpson, 2011; Wignall and Atkinson, 2020), and Early Jurassic (Han et al., 2018; Krencker et al., 2020; Han et al., 2022). The carbonate precipitation would prefer to incorporate the ^{24}Mg into the crystal lattices (Li et al., 2012, 2015), therefore, such a serious carbonate productivity crisis would lead to the reduction of ^{24}Mg sink and the decrease of seawater $\delta^{26}\text{Mg}$ values (Tipper et al., 2006; Hu et al., 2022b). However, the decline of the seawater $\delta^{26}\text{Mg}$ values as inferred from geological records is significantly rapid relative to the previous model-based prediction. This result implies that the Mg influx consumed by carbonate deposition was still overestimated, in other word, the carbonate productivity crisis perhaps was more serious than our present understanding. The potential triggers of carbonate productivity crises during these stages included sea-level fluctuations, enhanced terrigenous flux, and changes in microbial activities (Godet, 2013; Jin et al., 2018; Pálfy et al., 2021; Han et al., 2022; Jin et al., 2022). In the future, a quantitative estimation of carbonate production since the Late Triassic to Early Jurassic will provide more constraints to reassess the carbonate productivity crises.

6. Conclusions

- (1) As demonstrated by C isotopes and $^{87}\text{Sr}/^{86}\text{Sr}$ ratios, coeval seawater is the dolomitization fluid, providing the major Mg for the formation of dolomites. V/Cr, V/(V + Ni) ratios and Mn contents indicated that the carbonate in the BLC section deposited in the context of sea-level rise.
- (2) The dolomitization processes occurred at the high stands of sea level, during which an expanded platform could produce sufficient dolomitization fluid accounting for the pervasive dolomitization. The stratigraphic variation of $\delta^{26}\text{Mg}_{\text{dolo}}$ in the BLC section recorded the temporary basin restriction and the replenishment of seawater from the open ocean.
- (3) We run a numerical model to quantify the coupling effects of multistage dolomitization events on Mg isotope compositions of dolostones. Our results indicated, due to the most massive dolostone sequences formed in the “fluid-buffered” system, the multiple dolomitization processes homogenized the Mg isotope compositions along the sediment profile, erasing the environmental signals in carbonate.
- (4) We emphasize the importance to utilize multiple geochemical proxies to identify the most probable mechanisms influencing Mg isotopes of dolomites. Our presented $\delta^{26}\text{Mg}$ value of Early Jurassic seawater in this study is $\sim -0.5 \text{ ‰}$, which is significantly lower than the previous estimation.

CRediT authorship contribution statement

Zhongya Hu: Conceptualization, Funding acquisition, Investigation, Methodology, Project administration, Supervision, Writing – original draft, Writing – review & editing. **Zhong Han:** Funding acquisition, Writing – review & editing. **Anlin Ma:** Investigation, Writing – review & editing. **Zhiguang Xia:** Data curation, Formal analysis. **Lichao Wang:** Funding acquisition, Writing – review & editing. **Weiqiang Li:** Writing – original draft, Writing – review & editing.

Data availability

Data will be made available on request.

Declaration of competing interest

The authors declare that they have no known competing financial interests or personal relationships that could have appeared to influence the work reported in this paper.

Acknowledgments

We thank chief editor Prof. Brian Jones for the editorial handling. This manuscript benefits from constructive comments from two anonymous reviewers. This study is supported by the National Science Foundation of China (grants 42103004 and 42373005 to Z. Hu, 42272127 to L. Wang and 42002121 to Z. Han).

Appendix A. Supplementary data

Supplementary data to this article can be found online at <https://doi.org/10.1016/j.sedgeo.2023.106552>.

References

- Ahn, A.-S.C., Bjerrum, C.J., Blättler, C.L., Swart, P.K., Higgins, J.A., 2018. Quantifying early marine diagenesis in shallow-water carbonate sediments. *Geochimica et Cosmochimica Acta* 236, 140–159.
- Azmy, K., Lavoie, D., Wang, Z., Brand, U., Al-Aasm, I., Jackson, S., Girard, I., 2013. Magnesium-isotope and REE compositions of Lower Ordovician carbonates from eastern Laurentia: implications for the origin of dolomites and limestones. *Chemical Geology* 356, 64–75.
- Bennett, W.W., Canfield, D.E., 2020. Redox-sensitive trace metals as paleoredox proxies: a review and analysis of data from modern sediments. *Earth-Science Reviews* 204, 103175.
- Bialik, O.M., Wang, X., Zhao, S., Waldmann, N.D., Frank, R., Li, W., 2018. Mg isotope response to dolomitization in hinterland-attached carbonate platforms: Outlook of $\delta^{26}\text{Mg}$ as a tracer of basin restriction and seawater Mg/Ca ratio. *Geochimica et Cosmochimica Acta* 235, 189–207.
- Blättler, C.L., Miller, N.R., Higgins, J.A., 2015. Mg and Ca isotope signatures of authigenic dolomite in siliceous deep-sea sediments. *Earth and Planetary Science Letters* 419, 32–42.
- Budd, D.A., 1997. Cenozoic dolomites of carbonate islands: their attributes and origin. *Earth-Science Reviews* 42 (1–2), 1–47.
- Burdige, D.J., 1993. The biogeochemistry of manganese and iron reduction in marine sediments. *Earth-Science Reviews* 35 (3), 249–284.
- Chen, X.-Y., Teng, F.-Z., Sanchez, W.R., Romanek, C.S., Sanchez-Navas, A., Sánchez-Román, M., 2020. Experimental constraints on magnesium isotope fractionation during abiogenic calcite precipitation at room temperature. *Geochimica et Cosmochimica Acta* 281, 102–117.
- Demicco, R.V., Lowenstein, T.K., Hardie, L.A., Spencer, R.J., 2005. Model of seawater composition for the Phanerozoic. *Geology* 33, 877.
- Fantle, M.S., Higgins, J., 2014. The effects of diagenesis and dolomitization on Ca and Mg isotopes in marine platform carbonates: implications for the geochemical cycles of Ca and Mg. *Geochimica et Cosmochimica Acta* 142, 458–481.
- Fantle, M.S., Barnes, B.D., Lau, K.V., 2020. The role of diagenesis in shaping the geochemistry of the marine carbonate record. *Annual Review of Earth and Planetary Sciences* 48, 549–583.
- Fu, X., Wang, J., Feng, X., Wang, D., Chen, W., Song, C., Zeng, S., 2016a. Early Jurassic carbon-isotope excursion in the Qiangtang Basin (Tibet), the eastern Tethys: implications for the Toarcian Oceanic anoxic event. *Chemical Geology* 442, 62–72.
- Fu, X., Wang, J., Tan, F., Chen, M., Li, Z., Zeng, Y., Feng, X., 2016b. New insights about petroleum geology and exploration of Qiangtang Basin, northern Tibet, China: a model for low-degree exploration. *Marine and Petroleum Geology* 77, 323–340.
- Fu, X.G., Wang, J., Tan, F.W., Chen, M., Chen, W.B., 2010. The Late Triassic rift-related volcanic rocks from eastern Qiangtang, northern Tibet (China): age and tectonic implications. *Gondwana Research* 17 (1), 135–144.
- Geske, A., Zorlu, J., Richter, D.K., Buhl, D., Niedermayr, A., Immenhauser, A., 2012. Impact of diagenesis and low grade metamorphism on isotope ($\delta^{26}\text{Mg}$, $\delta^{13}\text{C}$, $\delta^{18}\text{O}$ and $^{87}\text{Sr}/^{86}\text{Sr}$) and elemental (Ca, Mg, Mn, Fe and Sr) signatures of Triassic sabkha dolomites. *Chemical Geology* 332, 45–64.
- Geske, A., Goldstein, R.H., Mavromatis, V., Richter, D.K., Buhl, D., Kluge, T., John, C.M., Immenhauser, A., 2015a. The magnesium isotope ($\delta^{26}\text{Mg}$) signature of dolomites. *Geochimica et Cosmochimica Acta* 149, 131–151.

- Geske, A., Lokier, S., Dietzel, M., Richter, D.K., Buhl, D., Immenhauser, A., 2015b. Magnesium isotope composition of sabkha porewater and related (sub-)recent stoichiometric dolomites, Abu Dhabi (UAE). *Chemical Geology* 393, 112–124.
- Godet, A., 2013. Drowning unconformities: palaeoenvironmental significance and involvement of global processes. *Sedimentary Geology* 293, 45–66.
- Gothmann, A.M., Stolarski, J., Adkins, J.F., Higgins, J.A., 2017. A Cenozoic record of seawater Mg isotopes in well-preserved fossil corals. *Geology* 45, 1039–1042.
- Gregg, J.M., Howard, S.A., Mazzullo, S.J., 1992. Early diagenetic recrystallization of Holocene (<3000 years old) peritidal dolomites, Ambergris Cay, Belize. *Sedimentology* 39 (1), 143–160.
- Hallam, A., 2001. A review of the broad pattern of Jurassic sea-level changes and their possible causes in the light of current knowledge. *Palaeogeography, Palaeoclimatology, Palaeoecology* 167 (1–2), 23–37.
- Han, Z., Hu, X., Li, J., Garzanti, E., 2016. Jurassic carbonate microfacies and relative sea-level changes in the Tethys Himalaya (southern Tibet). *Palaeogeography, Palaeoclimatology, Palaeoecology* 456, 1–20.
- Han, Z., Hu, X., Kemp, D.B., Li, J., 2018. Carbonate-platform response to the Toarcian Oceanic Anoxic Event in the southern hemisphere: implications for climatic change and biotic platform demise. *Earth and Planetary Science Letters* 489, 59–71.
- Han, Z., Hu, X., Hu, Z., Jenkyns, H.C., Su, T., 2022. Geochemical evidence from the Kioto Carbonate Platform (Tibet) reveals enhanced terrigenous input and deoxygenation during the early Toarcian. *Global and Planetary Change* 215, 103887.
- Hatch, J.R., Leventhal, J.S., 1992. Relationship between inferred redox potential of the depositional environment and geochemistry of the Upper Pennsylvanian (Missourian) Stark Shale Member of the Dennis Limestone, Wabaunsee County, Kansas, USA. *Chemical Geology* 99 (1–3), 65–82.
- Higgins, J.A., Schrag, D.P., 2010. Constraining magnesium cycling in marine sediments using magnesium isotopes. *Geochimica et Cosmochimica Acta* 74 (17), 5039–5053.
- Higgins, J.A., Schrag, D.P., 2015. The Mg isotopic composition of Cenozoic seawater—evidence for a link between Mg-clays, seawater Mg/Ca, and climate. *Earth and Planetary Science Letters* 416, 73–81.
- Higgins, J.A., Blättler, C.L., Lundstrom, E.A., Santiago-Ramos, D.P., Akhtar, A.A., Crüger Ahm, A.S., Bialik, O., Holmden, C., Bradbury, H., Murray, S.T., Swart, P.K., 2018. Mineralogy, early marine diagenesis, and the chemistry of shallow-water carbonate sediments. *Geochimica et Cosmochimica Acta* 220, 512–534.
- Hohl, S.V., Viehmann, S., 2021. Stromatolites as geochemical archives to reconstruct microbial habitats through deep time: potential and pitfalls of novel radiogenic and stable isotope systems. *Earth-Science Reviews* 218, 103683.
- Hu, X., Li, J., Han, Z., Li, Y., 2020. Two types of hyperthermal events in the Mesozoic-Cenozoic: environmental impacts, biotic effects, and driving mechanisms. *Science in China Series D: Earth Sciences* 63, 1041–1058.
- Hu, X., Ma, A., Xue, W., Garzanti, E., Cao, Y., Li, S.-M., Sun, G., Lai, W., 2022a. Exploring a lost ocean in the Tibetan Plateau: birth, growth, and demise of the Bangong-Nujiang Ocean. *Earth-Science Reviews* 229, 104031.
- Hu, Z., Hu, W., Wang, X., Lu, Y., Wang, L., Liao, Z., Li, W., 2017. Resetting of Mg isotopes between calcite and dolomite during burial metamorphism: outlook of Mg isotopes as geothermometer and seawater proxy. *Geochimica et Cosmochimica Acta* 208, 24–40.
- Hu, Z., Hu, W., Liu, C., Sun, F., Liu, Y., Li, W., 2019. Conservative behavior of Mg isotopes in massive dolostones: from diagenesis to hydrothermal reworking. *Sedimentary Geology* 381, 65–75.
- Hu, Z., Bialik, O.M., Hohl, S.V., Xia, Z., Waldmann, N.D., Liu, C., Li, W., 2021a. Response of Mg isotopes to dolomitization during fluctuations in sea level: constraints on the hydrological conditions of massive dolomitization systems. *Sedimentary Geology* 420, 105922.
- Hu, Z., Li, W., Zhang, H., Krainer, K., Zheng, Q.F., Xia, Z., Hu, W., Shen, S.Z., 2021b. Mg isotope evidence for restriction events within the Paleotethys ocean around the Permian-Triassic transition. *Earth and Planetary Science Letters* 556, 116704.
- Hu, Z., Shi, Z., Li, G., Xia, Z., Yi, L., Liu, C., Li, W., 2022b. The Cenozoic Seawater Conundrum: new constraints from Mg isotopes in island dolostones. *Earth and Planetary Science Letters* 595, 117755.
- Hu, Z., Hohl, S.V., Viehmann, S., Meister, P., Tepe, N., 2023. No biological effect on magnesium isotope fractionation during stromatolite growth. *Geochimica et Cosmochimica Acta* 358, 1–11.
- Huang, K.-J., Shen, B., Lang, X.-G., Tang, W.-B., Peng, Y., Ke, S., Kaufman, A.J., Ma, H.-R., Li, F.-B., 2015. Magnesium isotopic compositions of the Mesoproterozoic dolostones: implications for Mg isotopic systematics of marine carbonates. *Geochimica et Cosmochimica Acta* 164, 333–351.
- Immenhauser, A., 2022. On the delimitation of the carbonate burial realm. *The Depositional Record* 8 (2), 524–574.
- Jacobson, A.D., Zhang, Z., Lundstrom, C., Huang, F., 2010. Behavior of Mg isotopes during dedolomitization in the Madison Aquifer, South Dakota. *Earth and Planetary Science Letters* 297 (3–4), 446–452.
- Jin, X., Shi, Z., Rigo, M., Franceschi, M., Preto, N., 2018. Carbonate platform crisis in the Carnian (Late Triassic) of Hanwang (Sichuan Basin, South China): insights from conodonts and stable isotope data. *Journal of Asian Earth Sciences* 164, 104–124.
- Jin, X., Franceschi, M., Martini, R., Shi, Z., Gianolla, P., Rigo, M., Wall, C.J., Schmitz, M.D., Lu, G., Du, Y., Huang, X., Preto, N., 2022. Eustatic sea-level fall and global fluctuations in carbonate production during the Carnian Pluvial Episode. *Earth and Planetary Science Letters* 594, 117698.
- Jones, B., Manning, D.A., 1994. Comparison of geochemical indices used for the interpretation of palaeoredox conditions in ancient mudstones. *Chemical Geology* 111 (1–4), 111–129.
- Kasemann, S.A., von Strandmann, P.A.P., Prave, A.R., Fallick, A.E., Elliott, T., Hoffmann, K.H., 2014. Continental weathering following a Cryogenian glaciation: evidence from calcium and magnesium isotopes. *Earth and Planetary Science Letters* 396, 66–77.
- Kaufman, A.J., Jacobsen, S.B., Knoll, A.H., 1993. The Vendian record of Sr and C isotopic variations in seawater: implications for tectonics and paleoclimate. *Earth and Planetary Science Letters* 120 (3–4), 409–430.
- Kiessling, W., Simpson, C., 2011. On the potential for ocean acidification to be a general cause of ancient reef crises. *Global Change Biology* 17 (1), 56–67.
- Kimmig, S.R., Nadeau, M.D., Swart, P.K., Holmden, C., 2021. Mg and Sr isotopic evidence for basin wide alteration of early diagenetic dolomite in the Williston Basin by ascending crustal fluids. *Geochimica et Cosmochimica Acta* 311, 198–225.
- Krencker, F.N., Fantasia, A., Danisch, J., Martindale, R., Kabiri, L., El Ouali, M., Bodin, S., 2020. Two-phased collapse of the shallow-water carbonate factory during the late Pliensbachian-Toarcian driven by changing climate and enhanced continental weathering in the Northwestern Gondwana Margin. *Earth-Science Reviews* 208, 103254.
- Li, F.-B., Teng, F.-Z., Chen, J.-T., Huang, K.-J., Wang, S.-J., Lang, X.-G., Ma, H.-R., Peng, Y.-B., Shen, B., 2016. Constraining ribbon rock dolomitization by Mg isotopes: implications for the 'dolomite problem'. *Chemical Geology* 445, 208–220.
- Li, W., Chakraborty, S., Beard, B.L., Romanek, C.S., Johnson, C.M., 2012. Magnesium isotope fractionation during precipitation of inorganic calcite under laboratory conditions. *Earth and Planetary Science Letters* 333, 304–316.
- Li, W., Beard, B.L., Li, C., Xu, H., Johnson, C.M., 2015. Experimental calibration of Mg isotope fractionation between dolomite and aqueous solution and its geological implications. *Geochimica et Cosmochimica Acta* 157, 164–181.
- Li, W., Bialik, O.M., Wang, X., Yang, T., Hu, Z., Huang, Q., Zhao, S., Waldmann, N.D., 2019. Effects of early diagenesis on Mg isotopes in dolomite: the roles of Mn (IV)-reduction and recrystallization. *Geochimica et Cosmochimica Acta* 250, 1–17.
- Liu, C., Wang, Z., Raub, T.D., Macdonald, F.A., Evans, D.A., 2014. Neoproterozoic cap-dolostone deposition in stratified glacial meltwater plume. *Earth and Planetary Science Letters* 404, 22–32.
- Lumsden, D.N., Caudle, G.C., 2001. Origin of massive dolostone: the Upper Knox model. *Journal of Sedimentary Research* 71 (3), 400–409.
- Ma, A., Hu, X., Garzanti, E., Han, Z., Lai, W., 2017. Sedimentary and tectonic evolution of the southern Qiangtang basin: implications for the Lhasa-Qiangtang collision timing. *Journal of Geophysical Research – Solid Earth* 122 (7), 4790–4813.
- Ma, A., Hu, X., Kapp, P., Han, Z., Lai, W., BouDagher-Fadel, M., 2018a. The disappearance of a Late Jurassic remnant sea in the southern Qiangtang Block (Shamuluo Formation, Najiango area): Implications for the tectonic uplift of central Tibet. *Palaeogeography, Palaeoclimatology, Palaeoecology* 506, 30–47.
- Ma, H., Xu, Y., Huang, K., Sun, Y., Ke, S., Peng, Y., Lang, X., Yan, C., Shen, B., 2018b. Heterogeneous Mg isotopic composition of the early Carboniferous limestone: implications for carbonate as a seawater archive. *Acta Geochimica* 37, 1–18.
- Machel, H.G., Mountjoy, E.W., 1986. Chemistry and environments of dolomitization—a re-appraisal. *Earth-Science Reviews* 23 (3), 175–222.
- Mavromatis, V., Gautier, Q., Bosc, O., Schott, J., 2013. Kinetics of Mg partition and Mg stable isotope fractionation during its incorporation in calcite. *Geochimica et Cosmochimica Acta* 114, 188–203.
- Mavromatis, V., Purgstaller, B., Dietzel, M., Buhl, D., Immenhauser, A., Schott, J., 2017. Impact of amorphous precursor phases on magnesium isotope signatures of Mg-calcite. *Earth and Planetary Science Letters* 464, 227–236.
- Meister, P., Mckenzie, J.A., Bernasconi, S.M., Brack, P., 2013. Dolomite formation in the shallow seas of the Alpine Triassic. *Sedimentology* 60 (1), 270–291.
- Miller, K.G., Komínz, M.A., Browning, J.V., Wright, J.D., Mountain, G.S., Katz, M.E., Sugarman, P.G., Cramer, B.S., Christie-Blick, N., Pekar, S.F., 2005. The Phanerozoic record of global sea-level change. *Science* 310 (5752), 1293–1298.
- Ning, M., Huang, K., Lang, X., Ma, H., Yuan, H., Peng, Y., Shen, B., 2019. Can crystal morphology indicate different generations of dolomites? Evidence from magnesium isotopes. *Chemical Geology* 516, 1–17.
- Ning, M., Lang, X., Huang, K., Li, C., Huang, T., Yuan, H., Xing, C., Yang, R., Shen, B., 2020. Towards understanding the origin of massive dolostones. *Earth and Planetary Science Letters* 545, 116403.
- Pálfi, J., Kovács, Z., Demény, A., Vallner, Z., 2021. End-Triassic crisis and “unreefing” led to the demise of the Dachstein carbonate platform: a revised model and evidence from the Transdanubian Range, Hungary. *Global and Planetary Change* 199, 103428.
- Peng, Y., Shen, B., Lang, X.-G., Huang, K.-J., Chen, J.-T., Yan, Z., Tang, W.-B., Ke, S., Ma, H.-R., Li, F.-B., 2016. Constraining dolomitization by Mg isotopes: a case study from partially dolomitized limestones of the middle Cambrian Xuzhuang Formation, North China. *Geochemistry, Geophysics, Geosystems* 17 (3), 1109–1129.
- Petrash, D.A., Lalonde, S.V., González-Arismendi, G., Gordon, R.A., Méndez, J.A., Gingras, M.K., Konhauser, K.O., 2015. Can Mn-S redox cycling drive sedimentary dolomite formation? A hypothesis. *Chemical Geology* 404, 27–40.
- Petrash, D.A., Bialik, O.M., Bontognali, T.R., Vasconcelos, C., Roberts, J.A., McKenzie, J.A., Konhauser, K.O., 2017. Microbially catalyzed dolomite formation: from near-surface to burial. *Earth-Science Reviews* 171, 558–582.
- Qing, H., Mountjoy, E.W., 1994. Rare earth element geochemistry of dolomites in the Middle Devonian Presquile barrier, Western Canada Sedimentary Basin: implications for fluid-rock ratios during dolomitization. *Sedimentology* 41 (4), 787–804.
- Qing, H., Bosence, D.W., Rose, E.P., 2001. Dolomitization by penesaline sea water in Early Jurassic peritidal platform carbonates, Gibraltar, western Mediterranean. *Sedimentology* 48, 153–163.
- Qing, H., Qiao, Z., Zhang, S., Cosford, J., Hu, A., Liang, F., Wang, Y., Zheng, J., 2023. δ26Mg-δ13C-δ18O systems as geochemical tracers for dolomite recrystallization: a case study of lower Ordovician dolomite from Tarim Basin. *Chemical Geology* 619, 121302.
- Raczké, I., Jochum, K.P., Hofmann, A.W., 2003. Neodymium and strontium isotope data for USGS reference materials BCR-1, BCR-2, BHVO-1, BHVO-2, AGV-1, AGV-2, GSP-1, GSP-2 and eight MPI-DING reference glasses. *Geostandards and Geoanalytical Research* 27 (2), 173–179.
- Riechelmann, S., Mavromatis, V., Buhl, D., Dietzel, M., Eisenhauer, A., Immenhauser, A., 2016. Impact of diagenetic alteration on brachiopod shell magnesium isotope ($\delta^{26}\text{Mg}$) signatures: experimental versus field data. *Chemical Geology* 440, 191–206.

- Shao, L., Cui, Y., Qiao, P., Zhang, D., Liu, X., Zhang, C., 2017. Sea-level changes and carbonate platform evolution of the Xisha Islands (South China Sea) since the Early Miocene. *Palaeogeography, Palaeoclimatology, Palaeoecology* 485, 504–516.
- Su, N., Yang, S., Deng, K., Chang, Y.P., Xu, J., Wu, Z., 2021. Radiogenic and stable Sr isotopes constrain weathering processes in rapidly eroding Taiwan catchments. *Earth and Planetary Science Letters* 576, 117235.
- Sun, Y.D., Wignall, P.B., Joachimski, M.M., Bond, D.P.G., Grasby, S.E., Lai, X.L., Wang, L.N., Zhang, Z.T., Sun, S., 2016. Climate warming, euxinia and carbon isotope perturbations during the Carnian (Triassic) Crisis in South China. *Earth and Planetary Science Letters* 444, 88–100.
- Swart, P.K., 2015. The geochemistry of carbonate diagenesis: the past, present and future. *Sedimentology* 62 (5), 1233–1304.
- Tipper, E.T., Galy, A., Gaillardet, J., Bickle, M.J., Elderfield, H., Carder, E.A., 2006. The magnesium isotope budget of the modern ocean: constraints from riverine magnesium isotope ratios. *Earth and Planetary Science Letters* 250 (1–2), 241–253.
- Veizer, J., Ala, D., Azmy, K., Bruckschen, P., Buhl, D., Bruhn, F., Carden, G.A.F., Diener, A., Ebnet, S., Godderis, Y., Jasper, T., Korte, C., Pawellek, F., Podlaha, O.G., Strauss, H., 1999. ^{87}Sr / ^{86}Sr , $\delta^{13}\text{C}$ and $\delta^{18}\text{O}$ evolution of Phanerozoic seawater. *Chemical Geology* 161 (1–3), 59–88.
- Wang, J., Fu, X., Chen, W., Wang, Z., Tan, F., Chen, M., Zhuo, J., 2008. Chronology and geochemistry of the volcanic rocks in Woruo Mountain region, northern Qiangtang depression: Implications to the Late Triassic volcanic-sedimentary events. *Science China Earth Sciences* 51, 194–205.
- Wang, Y., Huang, C., Sun, B., Quan, C., Wu, J., Lin, Z., 2014. Paleo- CO_2 variation trends and the Cretaceous greenhouse climate. *Earth-Science Reviews* 129, 136–147.
- Wignall, P.B., Atkinson, J.W., 2020. A two-phase end-Triassic mass extinction. *Earth-Science Reviews* 208, 103282.
- Wilkinson, B.H., Algeo, T.J., 1989. Sedimentary carbonate record of calcium-magnesium cycling. *American Journal of Science* 289 (10), 1158–1194.
- Wilson, E.N., Hardie, L.A., Phillips, O.M., 1990. Dolomitization front geometry, fluid flow patterns, and the origin of massive dolomite; the Triassic Latemar buildup, northern Italy. *American Journal of Science* 290 (7), 741–796.
- Xue, W., Hu, X., Ma, A., Garzanti, E., Li, J., 2020. Eustatic and tectonic control on the evolution of the Jurassic North Qiangtang Basin, northern Tibet, China: impact on the petroleum system. *Marine and Petroleum Geology* 120, 104558.
- Zhang, F., Xu, H., Konishi, H., Roden, E.E., 2010. A relationship between $d\text{104}$ value and composition in the calcite-disordered dolomite solid-solution series. *American Mineralogist* 95, 1650–1656.
- Zhang, P., Huang, K.J., Luo, M., Cai, Y., Bao, Z., 2022. Constraining the terminal Ediacaran seawater chemistry by Mg isotopes in dolostones from the Yangtze Platform, South China. *Precambrian Research* 377, 106700.